

Single-shot and measurement-based quantum error correction via fault complexes

Timo Hillmann,^{1,2,*} Guillaume Dauphinais,¹ Ilan Tzitrin,^{1,†} and Michael Vasmer^{1,3,4}

¹*Xanadu, Toronto, Ontario, M5G 2C8, Canada*

²*Department of Microtechnology and Nanoscience (MC2),*

Chalmers University of Technology, SE-412 96 Gothenburg, Sweden

³*Perimeter Institute for Theoretical Physics, Waterloo, Ontario, N2L 2Y5, Canada*

⁴*Institute for Quantum Computing, Waterloo, Ontario, N2L 3G1, Canada*

(Dated: October 18, 2024)

Photonics provides a viable path to a scalable fault-tolerant quantum computer. The natural framework for this platform is measurement-based quantum computation, where fault-tolerant graph states supersede traditional quantum error-correcting codes. However, the existing formalism for foliation—the construction of fault-tolerant graph states—does not reveal how certain properties, such as single-shot error correction, manifest in the measurement-based setting. We introduce the fault complex, a representation of dynamic quantum error correction protocols particularly well-suited to describe foliation. Our approach enables precise computation of fault tolerance properties of foliated codes and provides insights into circuit-based quantum computation. Analyzing the fault complex leads to improved thresholds for three- and four-dimensional toric codes, a generalization of stability experiments, and the existence of single-shot lattice surgery with higher-dimensional topological codes.

Introduction.— Certain scalable platforms for fault-tolerant quantum computers, namely photonics [1–4], are particularly well-suited to the model of measurement-based quantum computation (MBQC) [5]. In this paradigm, in contrast to circuit-based quantum computation (CBQC), the central object is not a quantum error-correcting (QEC) code but a fault-tolerant graph state (FTGS). Various methods for constructing an FTGS exist [6–8], with the concept of foliation [9, 10] offering a prescription for any Calderbank-Shor-Steane (CSS) code [11, 12]. Here, we introduce the *fault complex*, a representation of faults in a dynamic QEC protocol rather than a static QEC code. We focus on fault complexes obtained via foliation, which we recast in the language of homology as a tensor product [13, 14] between a CSS code and a repetition code. This mathematical machinery allows us to exactly compute the properties of the QEC protocol, such as the fault distance, starting from any input CSS code. Our formalism is based on the representation of CSS codes as chain complexes [15, 16] and is related to distance balancing [17, 18]. Fault complexes also have an interpretation as repeated rounds of error correction over time in CBQC, allowing us to apply insights from our formalism to that domain. Analysis of the fault complex enables us to understand the decoding of single-shot codes in MBQC and achieve improved error thresholds for three-dimensional (3D) and 4D toric codes [19–22]. Through the explicit calculation of the homology groups of the fault complex, we generalize the notion of stability experiments [23], which in turn allows us to conclude that single-shot lattice surgery is possible in higher-dimensional topological codes.

Background and Notation.— An $[n, k, d]$ binary linear

code C forms a k -dimensional subspace within the n -dimensional vector space over \mathbb{F}_2 . Such a code can be defined by a parity-check matrix (PCM) H , where the codewords are the elements of $\ker H$. The distance d is the minimum Hamming weight of any nonzero codeword. We use e_i to denote the i^{th} unit vector and $[M]_j$ to denote the j^{th} row of a matrix M . We write $\mathbf{0}$ and $\mathbf{1}$ for the all-zero and all-one vectors, respectively.

A stabilizer code [24] is the quantum analogue of a linear code and is defined by an abelian subgroup, \mathcal{S} , of the Pauli group with $-I \notin \mathcal{S}$. The codespace is the $+1$ eigenspace of \mathcal{S} ; logical operators commute with \mathcal{S} but are not themselves in \mathcal{S} . The notation $[[n, k, d]]$ describes a code in which the stabilizer group is generated by $m = n - k$ independent generators, which are themselves elements of the n -qubit Pauli group \mathcal{P}_n . The number of encoded qubits is k and the distance d is determined by the minimum weight non-trivial logical operator. A stabilizer code admitting a set of stabilizer generators that are each either X -type or Z -type operators is referred to as a CSS code [11, 12]. These codes can be described by two classical binary linear codes with PCMs H_X and H_Z representing stabilizer generators as tensor products of X and I , and Z and I , respectively. Commutativity of X - and Z -type generators is expressed through the condition $H_Z^T H_X = 0$. Error correction proceeds via the measurement of the stabilizer generators, yielding the syndrome s , which is the list of stabilizer eigenvalues. This allows the detection and correction of Pauli errors that anti-commute with stabilizer generators; a classical decoder is used to infer recovery operators given a syndrome.

Here, a chain complex of length n denotes a collection of \mathbb{F}_2 -vector spaces C_i and linear maps ∂_i^C called boundary operators,

$$C = \{0\} \xrightarrow{\partial_{n+1}^C} C_n \xrightarrow{\partial_n^C} \dots \xrightarrow{\partial_2^C} C_1 \xrightarrow{\partial_1^C} C_0 \xrightarrow{\partial_0^C} \{0\}, \quad (1)$$

* timo.hillmann@rwth-aachen.de

† ilan@xanadu.ai

with the composition fulfilling $\partial_i^C \partial_{i+1}^C = 0$. We suppress superscripts if no distinction is necessary. Elements of the kernel $Z_i(\mathcal{C}) := \ker \partial_i$ are referred to as i -cycles, and elements of the image $B_i(\mathcal{C}) := \text{im } \partial_{i+1}$ as i -boundaries. The quotient $H_i(\mathcal{C}) := Z_i(\mathcal{C})/B_i(\mathcal{C}) = \ker \partial_i / \text{im } \partial_{i+1}$ is called the i^{th} homology group of \mathcal{C} . Associated with \mathcal{C} is also a cochain complex, with coboundary operators $\delta^i : C_i \rightarrow C_{i+1}$ defined as $\delta^i = \partial_{i+1}^T$:

$$\mathcal{C}^T = \{0\} \xrightarrow{\delta^{-1}} C_0 \xrightarrow{\delta^0} C_1 \xrightarrow{\delta^1} \dots \xrightarrow{\delta^{n-1}} C_n \xrightarrow{\delta^n} \{0\}. \quad (2)$$

Elements of $Z^i := \ker \delta^i$ and $B^i := \text{im } \delta^{i-1}$ are referred to as cocycles and coboundaries, respectively, and $H^i := \ker \delta^i / \text{im } \delta^{i-1}$ is the i^{th} cohomology group.

Each length-1 chain complex describes an $[n, k, d]$ linear code with boundary map $\partial_1 = H$ from the vector space \mathbb{F}_2^n to the space of syndromes \mathbb{F}_2^r with $r \geq n - k$. Similarly, a CSS code, \mathcal{C} , can be represented by a length-2 chain (sub)complex

$$\dots \rightarrow C_{i+1} \xrightarrow{\partial_{i+1}} C_i \xrightarrow{\partial_i} C_{i-1} \rightarrow \dots, \quad (3)$$

where, by convention, $\partial_{i+1} = H_Z^T$ and $\partial_i = H_X$, such that $\partial_i \partial_{i+1} = 0$ is encoded in the condition that $H_X H_Z^T = 0$. Identifying qubits with the space C_i , the code parameters are $n = \dim C_i$, $k = \dim H_i(\mathcal{C})$, and the logical operators are elements of the groups $H_i(\mathcal{C})$ and $H^i(\mathcal{C})$, with the smallest weight element defining d .

Fault Complexes.— We define a fault complex to be a length-3 chain (sub)complex \mathcal{F}

$$\dots \rightarrow F_{i+2} \xrightarrow{\partial_{i+2}} F_{i+1} \xrightarrow{\partial_{i+1}} F_i \xrightarrow{\partial_i} F_{i-1} \rightarrow \dots, \quad (4)$$

where we define *primal fault locations* to be elements of F_i and *dual fault locations* to be elements of F_{i+1} . The fault complex has $n = n_i + n_{i+1}$ total faults, where $n_i = \dim F_i$. The boundary map ∂_{i+1} determines equivalent primal and dual faults. We define the primal and dual *detector matrices* to be $D_X = \partial_i$ and $D_Z = \partial_{i+2}^T$, respectively. The syndrome of a primal fault $x \in F_i$ is $D_X x$ and the support of a primal detector $u \in F_{i-1}$ is $D_X^T u$, and similarly for dual faults and detectors. In a fault complex, there is no requirement for the commutativity of the primal and dual detector matrices. Instead, we have $\partial_i \partial_{i+1} = 0$, meaning that a primal fault that is equivalent to a dual fault has trivial (primal) syndrome, with an analogous interpretation for $\partial_{i+2}^T \partial_{i+1}^T = 0$.

We refer to the elements of $H^i(\mathcal{F})$ and $H_{i+1}(\mathcal{F})$ as primal and dual *logical correlations*, respectively. These represent the information that the fault complex is designed to protect. Similarly, the elements of $H_i(\mathcal{F})$ and $H^{i+1}(\mathcal{F})$ are the primal and dual *logical errors*, respectively. These operators change the values of the logical correlations but have no syndrome and are therefore undetectable. Note that the number of primal logical correlations (or errors) $k_i = \dim H^i(\mathcal{F}) = \dim H_i(\mathcal{F})$ need not equal the number of dual logical correlations (or errors) $k_{i+1} = \dim H_{i+1}(\mathcal{F}) = \dim H^{i+1}(\mathcal{F})$. The primal (dual)

fault distance d_i (d_{i+1}) of the fault complex is the weight of the minimal weight primal (dual) logical error.

Recently, there have been many proposals for formalizing fault-tolerant protocols [7, 8, 25–32], some of which bear some resemblance to fault complexes. In particular, our definition of a fault complex builds on the definition of a *fault-tolerant cluster state* in [8]. We also note that fault complexes are distinct from the *fault-tolerant complexes* of [29], which are defined geometrically and are limited to topological codes. Fault complexes have an interpretation in CBQC where the faults can represent both qubit, gate, and measurement errors. In this interpretation, ∂_{i+1} is related to the gauge group of the spacetime code; see Appendix F for a further discussion. Here, we concentrate on the interpretation of fault complexes in MBQC, where they give a useful representation of foliated codes.

Fault Complexes of Foliated Codes.— A common way to obtain an FTGS from a CSS code is through foliation [9]. In this procedure, the X and Z Tanner graphs of the code are interpreted as alternating layers of the FTGS, and data qubits between adjacent layers are entangled with each other; see Fig. 1(a-d). The computation is then performed by a sequence of adaptive local measurements on the FTGS. We now show that foliation can be algebraically formulated as the tensor (or hypergraph [13, 14]) product of a base CSS code with a repetition code, yielding a fault complex. As a result, the detectors, logical correlations/errors, and fault distances of the fault complex can be directly calculated from the base code.

Let \mathcal{C} be the chain complex describing a CSS code and let \mathcal{R} be a length-1 chain complex describing a binary linear code. We obtain the fault complex as the product complex $\mathcal{F} = \mathcal{R} \times \mathcal{C}$. The fault complex has spaces

$$F_j = \bigoplus_{\ell+m=j} R_\ell \otimes C_m \quad (5)$$

where R_ℓ and C_m are the ℓ^{th} and m^{th} spaces of \mathcal{R} and \mathcal{C} , respectively. The boundary operators of the fault complex are

$$\partial_j = \left(\begin{array}{c|c} \mathbb{1}_r \otimes \partial_j^C & R \otimes \mathbb{1}_{n_{j-1}^C} \\ \hline 0 & \mathbb{1}_c \otimes \partial_{j-1}^C \end{array} \right), \quad (6)$$

where ∂_j^C is the j^{th} boundary operator of \mathcal{C} , and R is the $r \times c$ PCM of the binary linear code. See Fig. 1(e) for a diagrammatic representation of the fault complex vector space and boundary maps. From the Künneth formula, we obtain the number of primal and correlations

$$k_i = \dim H_0(\mathcal{R}) \dim H_i(\mathcal{C}) + \dim H_1(\mathcal{R}) \dim H_{i-1}(\mathcal{C}), \\ k_{i+1} = \dim H_0(\mathcal{R}) \dim H_{i+1}(\mathcal{C}) + \dim H_1(\mathcal{R}) \dim H_i(\mathcal{C}).$$

One can show [14, and Appendix B] that the primal and dual fault distances of \mathcal{F} are given by

$$d_i = \min[d_0(\mathcal{R})d_i(\mathcal{C}), d_1(\mathcal{R})d_{i-1}(\mathcal{C})], \\ d_{i+1} = \min[d_0(\mathcal{R}^T)d_{i+1}(\mathcal{C}^T), d_1(\mathcal{R}^T)d_i(\mathcal{C}^T)], \quad (7)$$

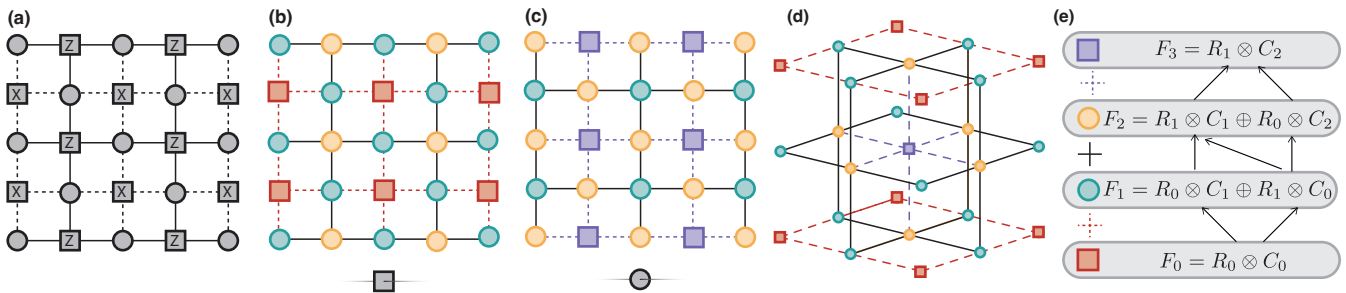


FIG. 1. Foliation of the surface code viewed as a fault complex. **(a)** The distance-3 surface code Tanner graph with circles representing qubits, squares with appropriate labels representing X and Z checks, and dashed and solid lines representing the connectivity of these checks, respectively. **(b)** and **(c)** Hypergraph product of **(a)** with a repetition code check and bit node, respectively. This yields two types of fault locations, teal and yellow, along with primal (red) and dual (purple) detectors. Dashed and solid lines indicate boundary maps of the fault complex. For simplicity, we omit out-of-plane connections. **(d)** Unit cell of the fault complex obtained by stacking alternating layers of **(b)** and **(c)**. A dual detector (purple) is formed by the parity of six dual fault locations (yellow). Vertical red dashed lines are omitted for clarity. **(e)** Mathematical structure of the fault complex and its relation to **(b)**-**(d)**: colored circles and squares are associated with chain complex vector spaces and lines are associated with boundary maps.

where $d_i(\mathcal{C})$ and $d_i(\mathcal{C}^T)$ are equal to the minimal weight of an element in $H_i(\mathcal{C})$ and $H^i(\mathcal{C})$, respectively. For trivial homology groups the associated distance is defined as ∞ .

Example: CSS codes.— Suppose that \mathcal{R} describes a repetition code with PCM R and distance δ , and that \mathcal{C} is a length-2 chain complex describing a CSS code with PCMs H_X and H_Z . Further, we assume that R , H_X , and H_Z are full rank. The nontrivial boundary operators, $\partial_j, j \in \{1, 2, 3\}$, of the fault complex $\mathcal{F} = \mathcal{R} \times \mathcal{C}$ can be explicitly obtained from Eq. (6). In particular, the rows of ∂_1 describe the support of primal detectors; they are all of the form $(e_\alpha \otimes [H_X]_\beta | [R]_\alpha \otimes e_\beta)$, with an analogous form for the columns of ∂_3 . These are exactly the foliated stabilizers of [9]; see Fig. 1(d), which illustrates a dual detector. Each detector (row) above is triggered by a fault on one of the qubits participating in the check $[H_X]_\beta$, or by a syndrome fault in the previous or next layer. The logical correlations are recovered from the homology group, that is, for example,

$$\begin{aligned} H_2(\mathcal{F}) &\cong H_0(\mathcal{R}) \otimes H_2(\mathcal{C}) \oplus H_1(\mathcal{R}) \otimes H_1(\mathcal{C}) \\ &= \langle (\mathbf{0}, \mathbf{1} \otimes \ell_Z) \mid \ell_Z \in \ker H_X / \text{im } H_Z^T \rangle, \end{aligned} \quad (8)$$

where \cong denotes isomorphic to and ℓ_Z is a logical Z operator of the base code. See Appendix B for a detailed derivation. This operator is a dual logical correlation; it acts as a copy of the logical Z operator on the qubits in the $R_1 \otimes C_1$ block of the F_1 space. The dual logical errors are given by

$$\begin{aligned} H^2(\mathcal{F}) &\cong H^0(\mathcal{R}) \otimes H^2(\mathcal{C}) \oplus H^1(\mathcal{R}) \otimes H^1(\mathcal{C}) \\ &= \langle (\mathbf{0}, (1, 0, \dots, 0) \otimes \ell_X) \mid \ell_X \in \ker H_Z / \text{im } H_X^T \rangle, \end{aligned} \quad (9)$$

where ℓ_X is a logical X operator of the base code. We observe that this operator acts as a logical X operator on one of the factors in the $R_1 \otimes C_1$ portion of the F_1 space. Applying Eq. (7), we find that the (dual) fault distance

of \mathcal{F} is $d_2 = d_X$, where d_X is the X -distance of the base code.

For our choice of \mathcal{R} , the homology groups $H_0(\mathcal{R})$ and $H^0(\mathcal{R})$ are trivial, so the fault complex lacks primal logical correlations arising from the base code's logical Z . This may seem surprising, given that the foliated surface code can be used to prepare an encoded Bell state on the two boundaries [33]. There is no contradiction, however: the interpretation of fault complexes as foliated codes implicitly assumes that all qubits are measured in the X basis during the protocol, and therefore that the encoded Bell state of [33] is measured destructively. The analogous CBQC interpretation is of a memory experiment with logical state preparation and readout both performed in the Z basis. In addition, we note that all the logical correlations can be recovered by considering an alternative repetition code PCM (see Appendix B).

Stability experiments.— Now suppose that H_X of the base code \mathcal{C} is rank deficient. The fault complex $\mathcal{F} = \mathcal{R} \times \mathcal{C}$ now has additional logical correlations and errors coming, respectively, from the following homology groups

$$\begin{aligned} H^1(\mathcal{F}) &\cong \langle (\mathbf{0}, (1, 0, \dots, 0) \otimes g) \mid g \in \ker H_X^T \rangle, \\ H_1(\mathcal{F}) &\cong \langle (\mathbf{0}, \mathbf{1} \otimes h) \mid h \in C_0 / \text{im } H_X \rangle \end{aligned} \quad (10)$$

Here, g represents any subset of H_X rows that sum to zero and h is any vector in C_0 that is not the syndrome of a Z -type error. An example of such a code is a 2D surface code with four smooth boundaries; in this case we have $g = \mathbf{1}$ (the product of all X stabilizers is I) and $h = (1, 0, \dots, 0)$ (all valid syndromes have even weight). Note that g is exactly the global spacelike invariant considered in stability experiments [23], which can be used to estimate the expected logical error when performing lattice surgery [34, 35], a method for performing logical operations via measurements. Using Eq. (7) we find that the primal distance of \mathcal{F} is $d_1 = \delta$, i.e., equal the distance of the repetition code (or the number of CBQC

measurement rounds cf. [23]). A 2D surface code with four smooth boundaries encodes no logical qubits, but if instead we let \mathcal{C} be the 2D toric code (with periodic boundaries) then our formalism shows that the fault complex $\mathcal{F} = \mathcal{R} \times \mathcal{C}$ can be used to perform a combined memory and stability experiment.

Single-shot lattice surgery.— Certain CSS codes are naturally associated with length-3 or length-4 chain complexes, where the additional vector spaces represent metachecks, i.e., redundancies between subsets of checks. Metachecks are related to single-shot error correction [21, 36, 37], where a single round of parity-check measurements suffices for fault-tolerant QEC.

As a prototypical example of a code with metachecks, let \mathcal{C} represent the 3D toric code [19, 20] defined on an $L \times L \times L$ cubic tiling, which has single-shot QEC for Z errors. We focus on this code for ease of presentation, but our results also hold for true single-shot CSS codes such as the 4D toric code. We assign the metacheck matrix $M_X = \partial_1^C$ and PCMs $H_X = \partial_2^C$ and $H_Z = (\partial_3^C)^T$. The primal detectors of the fault complex $\mathcal{F} = \mathcal{R} \times \mathcal{C}$ are given by ∂_2 , which now contains the metachecks; see Appendix C for the explicit expression. We note that \mathcal{F} is effectively a length-3 chain complex exactly because ‘data’ and ‘measurement’ faults are treated on an equal footing.

The expression for the primal logical correlations and errors of \mathcal{F} is the same as Eq. (10), but now with $g \in \ker H_X^T / \text{im } M_X^T$ and $h \in \ker M_X / \text{im } H_X$. As in the previous example, g is the logical correlation relevant for stability experiments and lattice surgery, and h is the logical error that can disrupt this correlation. In the 3D toric code, there are three independent choices of g given by all edges cutting through one of the independent 2D planes of the tiling. The corresponding h vectors correspond to non-contractible chains of edges along one of the coordinate axes of the tiling. As a result, all choices of h have extensive weight, i.e., $|h| \geq L$. Thus, even for a fault complex formed using a constant-length repetition code, a macroscopic number of faults ($\sim L$) is necessary to disrupt the g logical correlations. This is captured by the primal fault distance of \mathcal{F} , $d_1 = \delta L$, where $\delta = d_1(\mathcal{R})$ is the distance of the repetition code. Therefore, higher dimensional topological codes such as the 3D and 4D toric codes are compatible with *single-shot lattice surgery*, though at the cost of reduced performance. Counter-intuitively, the full distance can be restored in those cases by choosing \mathcal{R} such that $\delta = L = O(\sqrt{d})$, (where d is the distance of the code), or equivalently by performing $O(\sqrt{d})$ rounds of stabilizer measurement in the lattice surgery protocol. This should be contrasted with the 2D toric code case where the number of measurement rounds must be $O(d)$. Thus, we expect that a fault-tolerant quantum computing architecture based on the 4D toric code would have an asymptotic spacetime overhead reduction when compared to the standard 2D toric code architecture.

We address the case of single-shot codes with rank-

deficient PCMs without metachecks in Appendix B. We note that there exist single-shot quantum codes with full-rank PCMs [38, 39], to which our arguments above cannot be applied, and the existence of single-shot lattice surgery protocols for these codes remains an open question. We conjecture that codes enabling single-shot lattice surgery without performance degradation can be constructed from the balanced product of two good qLDPC codes [40–44].

Improved decoding of single-shot codes.— Estimating the error threshold of a single-shot code requires simulating multiple rounds of noisy syndrome measurement until the threshold has converged [45]. Since in MBQC there always exist detectors spanning multiple rounds, decoding must proceed using an overlapping window decoder [19, 46–49], which is naturally defined for a fault complex. A (w, c) -overlapping window decoder determines in each round a correction for a window of $w \in \mathbb{N}^+$ rounds and commits a correction to $c \leq w$ rounds (see Refs. [48, 50] for a more detailed description). Here, one round constitutes a check node and a bit node layer; see Fig. 1. For the 3D toric code, the effective distance of the decoding window then becomes $\min(wL, L^2)$, see Appendix B. However, wL is the weight of time-like logical errors and in this section we consider memory experiments, i.e., only space-like logical errors cause logical failures (see the End Matter for stability experiment simulations). State-of-the-art results in decoding higher-dimensional topological codes [22] employ a single-stage decoding approach that is recovered using a $(1, 1)$ -overlapping window decoder, see Appendix D. We find that increasing w to 2 or 3 significantly increases the sustainable threshold of 3D and 4D toric codes compared to $w = 1$ when using belief propagation (BP) plus ordered statistics decoding (OSD) [51, 52]; see Appendix D for details concerning the simulations. For $w = 3$, the thresholds for phenomenological Pauli noise of approximately 9.65% (3D) and 5.9% (4D) surpass all previous results [21, 22, 53–58], approaching the thresholds achieved with the optimal window choice $w = L$, see Fig. 2(a) and Fig. 2(c). We note that for the 3D toric code, we only consider primal faults, as the dual side of the fault complex does not have the single-shot property.

Additionally, we investigated the threshold under a noise model for Xanadu’s photonic architecture based on Gottesman-Kitaev-Preskill (GKP) qubits [1, 2, 59], with cluster state construction and error model details provided in [4]. For the 4D toric code, we observe a threshold of approximately 10.35 dB, comparable to that of the 2D variant [1, 2]. The 3D code achieves a threshold of approximately 7.95 dB. In both cases, the $w = 3$ decoder archives thresholds comparable to the $w = L$ decoder, see Fig. 2(b) and Fig. 2(d).

While larger decoding regions increase decoding time, recent advances provide solutions. Findings on localized statistics decoding [60], a parallelizable OSD variant, and on belief propagation for higher-dimensional toric codes [61] suggest time-efficient decoding with minimal

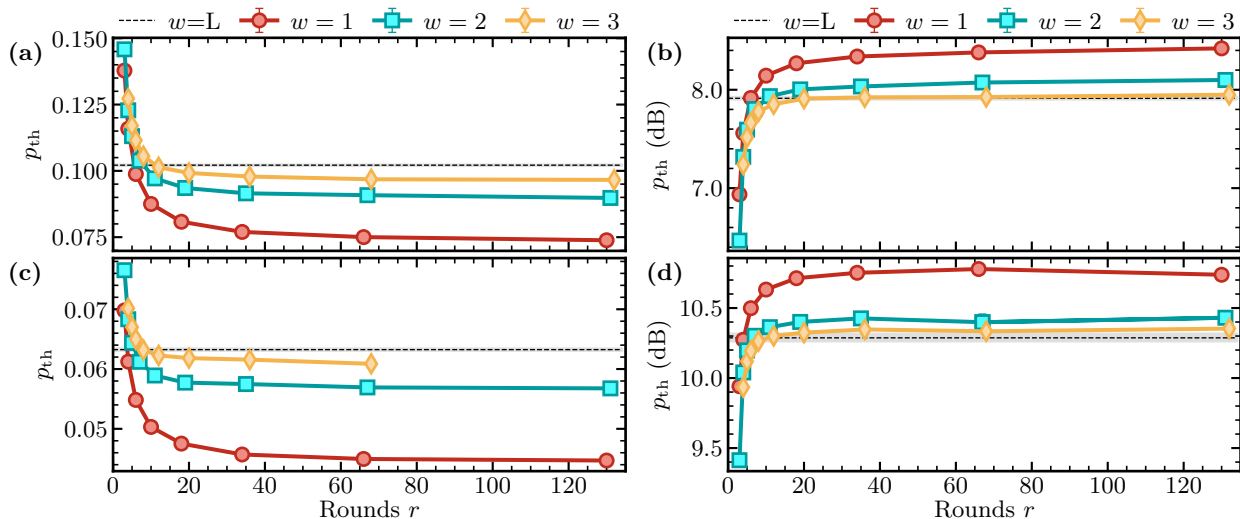


FIG. 2. Sustainable thresholds for 3D (top row) and 4D (bottom row) toric codes under two noise models: phenomenological Pauli noise (left column) and a noise model for a photonic GKP-based architecture (right column). Markers represent the threshold for a $(w, 1)$ -overlapping window decoder as a function of noisy syndrome rounds. The black dashed line shows the threshold from the optimal window choice $w = L$; see Appendix D for details. In the 3D case we only consider primal faults, whereas in the 4D case we consider both primal and dual faults.

performance reduction, supporting the practical applicability of our results.

Conclusion.— We introduced fault complexes, which represent dynamic QEC protocols and provide a convenient characterization of foliated codes. Through the explicit calculation of the homology groups of the fault complex, we gained insights into stability experiments and lattice surgery, and we derived improved decoding protocols for higher-dimensional topological codes such as the 4D toric code. The increased threshold values and asymptotic space-time advantage warrant serious consideration of the practical implementation of the 4D code in potentially compatible architectures such as photonics [1–3], trapped ions [62] or neutral atoms [63]. Algorithmic fault tolerance [64] offers asymptotically lower overhead, but it demands complex, correlated decoding. In contrast, the 4D toric code is more amenable to windowed decoding, and while the formal analysis requires decoding over $O(\sqrt{d})$ rounds, our numerical findings indicate that fewer layers might suffice in practice (see also [47]). On an intermediate time scale, the lower threshold requirements of 3D toric codes make them a promising experimental candidate to validate noise models and expected performance.

On a broader scale, it is worth exploring what MBQC can teach us about CBQC, e.g., by extending our formalism to circuit-level noise. Reformulating Li’s [32] LDPC representation of fault-tolerant quantum circuits is potentially straightforward in our approach, as many of their results in [32, Sec. VIII] are already structurally equivalent to Eq. (6). It would also be interesting to explore the extension of our formalism to subsystem codes [65–67], especially those with single-shot error cor-

rection [36, 45, 68]. Additionally, symplectic chain complexes may be explored to further incorporate non-CSS codes. See Appendix E for some ideas on these extensions.

We applied our formalism to foliation, i.e., constructing fault complexes using tensor products of chain complexes. In future work, we plan to investigate alternative product constructions of fault complexes using, e.g., the balanced product [43] and the lifted product [69]. Given that these products are known to yield CSS codes with optimal parameters [42], they may also yield improved fault complexes. In addition, by using alternative linear codes in the fault complex construction, we may hope to algebraically recover FTGS beyond foliation [7, 29].

ACKNOWLEDGMENTS

Acknowledgments.— The authors would like to thank Ben Brown, Christopher Chubb, Austin Daniel, Arthur Pesah, Alex Townsend-Teague, and Dominic Williamson for insightful discussions. We thank Rafael Alexander, J. Eli Bourassa, and Eric Sabo for feedback on an earlier draft of this manuscript. Research at Perimeter Institute is supported in part by the Government of Canada through the Department of Innovation, Science and Economic Development Canada and by the Province of Ontario through the Ministry of Colleges and Universities. Computations were performed on the Niagara supercomputer at the SciNet HPC Consortium. SciNet is funded by Innovation, Science and Economic Development Canada; the Digital Research Alliance of Canada; the Ontario Research Fund: Research Excellence; and

the University of Toronto.

Appendix A: End Matter

Stability Experiments.— To further support our claim that 3D and 4D toric codes are compatible with single-shot lattice surgery, we perform simulations of stability experiments. Stability experiments can be used as a proxy for simulating lattice surgery because they probe the accuracy of reliably inferring the outcomes of an extensive number of stabilizers [23]. We perform numerical simulations over 32 decoding rounds for a 3D toric code of linear size L (with periodic boundaries in time to avoid finite-size effects). In this case, the corresponding fault complex is equivalent to the chain complex that describes an asymmetric 4D toric code with dimensions $L \times L \times L \times w$ for each decoding window. As described in the main text and in Appendix D, decoding proceeds with an $(w, 1)$ overlapping window decoder. In this case, the effective primal fault distance is $d_1 = wL$, i.e., for $w \leq L$ the distance is limited by the size of the decoding window. But even for $w = 1$ we expect to observe an error threshold based on the distance scaling $d \sim L$. The $w = 1$ case corresponds to single-shot lattice surgery, but we note that any $w = O(1)$ corresponds to constant time overhead lattice surgery. Our results are summarized in Fig. 3. As expected from the distance calculation, we observe an error threshold for all values of w , with the logical error rate decreasing with increasing L below the threshold. By increasing the decoding window size w from $w = 1$ in Fig. 3(a), to larger, but constant, values of $w = 2$ in Fig. 3(b) and $w = 3$ in Fig. 3(c) we observe increased error thresholds in the stability experiments. We note that choosing w adaptively on the code size, e.g., $w = L$ balances time-like and space-like errors. In practice, this allows one to find a trade-off between the number of syndrome measurement rounds required for lattice surgery, and thus the time overhead for logical gates, and the achievable logical error rates of the gate. We emphasize that these observations are in stark contrast to stability experiments with non-single shot codes, as performed by Gidney [23] on the 2D surface code, where the effective distance is independent of L . For two codes with $L_2 > L_1$, the code with L_1 will always have a lower error rate than the code with L_2 if decoded over the same window size w .

Appendix B: Derivation of logical correlations and errors

Here we derive the expressions for logical errors/correlations and fault distances given in the main text and discuss their interpretation in more detail. We consider the fault complex $\mathcal{F} = \mathcal{R} \times \mathcal{C}$, where \mathcal{C} describes a CSS code and \mathcal{R} describes the repetition code whose parity-check matrix has a redundant row[70], as the main

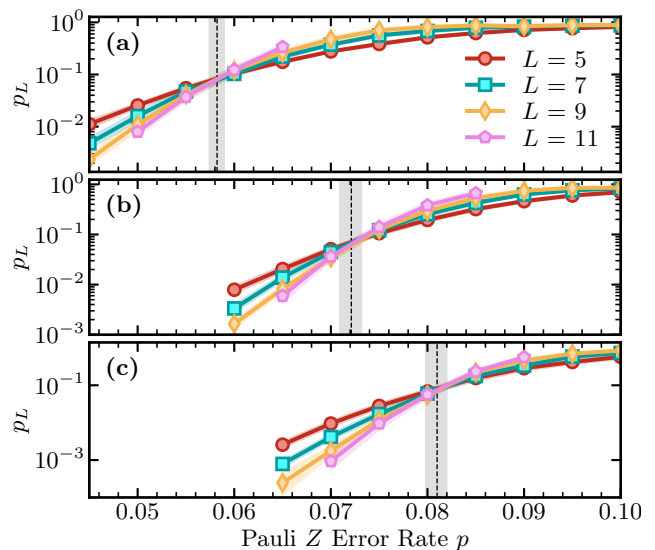


FIG. 3. Logical error rate for the time-like logical correlation of a 3D toric code for different window sizes of the overlapping window decoder. In (a) $w = 1$, (b) $w = 2$, and (c) $w = 3$. Vertical black dashed lines indicate the fitted threshold. The shading indicates a confidence interval, indicating hypotheses whose likelihoods are within a factor of 1000 of the maximum likelihood estimate.

text considers a special case of this. Explicitly,

$$R = \begin{bmatrix} 1 & 1 & 0 & \dots & 0 & 0 \\ 0 & 1 & 1 & \dots & 0 & 0 \\ \vdots & & & \ddots & & \vdots \\ 0 & 0 & 0 & \dots & 1 & 1 \\ 1 & 0 & 0 & \dots & 0 & 1 \end{bmatrix}. \quad (\text{B1})$$

We will refer to the i^{th} boundary operator of \mathcal{C} by ∂_i to ease notational clutter.

To obtain the homology groups of the fault complex, we make use of the Künneth formula:

$$H_j(\mathcal{F}) \cong H_0(\mathcal{R}) \otimes H_j(\mathcal{C}) \oplus H_1(\mathcal{R}) \otimes H_{j-1}(\mathcal{C}). \quad (\text{B2})$$

Similarly, for the cohomology groups, we have

$$H^j(\mathcal{F}) \cong H^0(\mathcal{R}) \otimes H^j(\mathcal{C}) \oplus H^1(\mathcal{R}) \otimes H^{j-1}(\mathcal{C}). \quad (\text{B3})$$

For \mathcal{R} , one can verify that

$$\begin{aligned} H_0(\mathcal{R}) &= R_0 / \text{im } R, \\ H_1(\mathcal{R}) &= \ker R / \{0\} \cong \ker R, \\ H^0(\mathcal{R}) &= \ker R^T / \{0\} \cong \ker R^T, \\ H^1(\mathcal{R}) &= R_1 / \text{im } R^T, \end{aligned} \quad (\text{B4})$$

Further calculation shows that

$$\begin{aligned} \text{im } R &= \text{im } R^T \\ &= \text{span}\{(1, 1, 0, \dots, 0), \dots, (0, \dots, 0, 1, 1)\} \end{aligned} \quad (\text{B5})$$

and $\ker R = \ker R^T = \{\mathbf{0}, \mathbf{1}\}$. Therefore

$$\begin{aligned} H_0(\mathcal{R}) &\cong \{\mathbf{0}, (1, 0, \dots, 0)\}, \\ H_1(\mathcal{R}) &\cong \{\mathbf{0}, \mathbf{1}\}, \\ H^0(\mathcal{R}) &\cong \{\mathbf{0}, \mathbf{1}\}, \\ H^1(\mathcal{R}) &\cong \{\mathbf{0}, (1, 0, \dots, 0)\}. \end{aligned} \quad (\text{B6})$$

Using Eqs. (B2) and (B6) we have

$$\begin{aligned} H_i(\mathcal{F}) &\cong H_0(\mathcal{R}) \otimes H_i(\mathcal{C}) \oplus H_1(\mathcal{R}) \otimes H_{i-1}(\mathcal{C}) \\ &= \langle \langle (1, 0, \dots, 0) \otimes \ell_Z, \mathbf{0} \rangle, (\mathbf{0}, \mathbf{1} \otimes h) \rangle, \end{aligned} \quad (\text{B7})$$

where $\ell_Z \in \ker \partial_i / \text{im } \partial_{i+1}$ and $h \in \ker \partial_{i-1} / \text{im } \partial_i$. Similarly, we have

$$\begin{aligned} H^i(\mathcal{F}) &\cong H^0(\mathcal{R}) \otimes H^i(\mathcal{C}) \oplus H^1(\mathcal{R}) \otimes H^{i-1}(\mathcal{C}) \\ &= \langle \langle (\mathbf{1} \otimes \ell_X, \mathbf{0}) \rangle, (\mathbf{0}, (1, 0, \dots, 0) \otimes g) \rangle, \end{aligned} \quad (\text{B8})$$

where $\ell_X \in \ker \partial_{i+1}^T / \text{Im } \partial_i^T$ and $g \in \ker \partial_i^T / \text{im } \partial_{i-1}^T$. We refer to elements of $H^i(\mathcal{C})$ as primal logical correlations and to elements of $H_i(\mathcal{C})$ as primal logical errors. Analogously for the other relevant homology groups, we have

$$\begin{aligned} H_{i+1}(\mathcal{F}) &\cong H_0(\mathcal{R}) \otimes H_{i+1}(\mathcal{C}) \oplus H_1(\mathcal{R}) \otimes H_i(\mathcal{C}) \\ &= \langle \langle (1, 0, \dots, 0) \otimes g', \mathbf{0} \rangle, (\mathbf{0}, \mathbf{1} \otimes \ell'_Z) \rangle, \end{aligned} \quad (\text{B9})$$

where $g' \in \ker \partial_{i+1} / \text{im } \partial_{i+2}$ and $\ell'_Z \in \ker \partial_i / \text{im } \partial_{i+1}$. And

$$\begin{aligned} H^{i+1}(\mathcal{F}) &\cong H^0(\mathcal{R}) \otimes H^{i+1}(\mathcal{C}) \oplus H^1(\mathcal{R}) \otimes H^i(\mathcal{C}) \\ &= \langle \langle (\mathbf{1} \otimes h', \mathbf{0}) \rangle, (\mathbf{0}, (1, 0, \dots, 0) \otimes \ell'_X) \rangle, \end{aligned} \quad (\text{B10})$$

where $h' \in \ker \partial_{i+2}^T / \text{im } \partial_{i+1}^T$ and $\ell'_X \in \ker \partial_{i+1}^T / \text{im } \partial_i^T$. We refer to the elements of $H_{i+1}(\mathcal{F})$ as dual logical correlations and to $H^{i+1}(\mathcal{F})$ as dual logical errors.

Recall that the number of primal and dual logical correlations (or errors) of a fault complex are defined to be $k_i = \dim H_i(\mathcal{F})$ and $k_{i+1} = \dim H_{i+1}(\mathcal{F})$, respectively. Using Eq. (B2), we obtain the general expression for these quantities

$$\begin{aligned} k_i &= \dim H_0(\mathcal{R}) \dim H_i(\mathcal{C}) + \dim H_1(\mathcal{R}) \dim H_{i-1}(\mathcal{C}), \\ k_{i+1} &= \dim H_0(\mathcal{R}) \dim H_{i+1}(\mathcal{C}) + \dim H_1(\mathcal{R}) \dim H_i(\mathcal{C}), \end{aligned}$$

which in our case further simplifies via Eq. (B6) giving

$$\begin{aligned} k_i &= \dim H_i(\mathcal{C}) + \dim H_{i-1}(\mathcal{C}), \\ k_{i+1} &= \dim H_{i+1}(\mathcal{C}) + \dim H_i(\mathcal{C}), \end{aligned} \quad (\text{B11})$$

We see that $k_i \neq k_{i+1}$ in general, with equality only when $\dim H_{i-1} = \dim H_{i+1}$.

Let us now consider the interpretation of the logical correlations and errors in terms of the CSS code described by \mathcal{C} . We concentrate on the primal case as the dual case is analogous. Note that each ℓ_Z describes the support of a logical Z operator (of the CSS code) and each ℓ_X describes the support of a logical X operator. Therefore, symplectic pairs of logical operators in the CSS code lift

to symplectic pairs of logical correlations and errors in the fault complex. If ∂_i is full rank, then $\text{im } \partial_i = C_{i-1}$ and $\ker \partial_i^T = \{\mathbf{0}\}$. In this case, the only possible choices for g and h are the zero vector, and therefore the generators of the homology groups all derive from the logical operators of the CSS code. Now suppose that C_i is rank deficient. In this case, g describes a subset of X -type stabilizer generators whose product is the identity, but which is not an X -type meta-check of the code. And h is a vector in C_{i-1} with trivial meta-syndrome, but which is not the syndrome of a Z -type error (see the main text for an example). If the code does not have X -type meta-checks (i.e., \mathcal{C} is length-2) then g can be any subset of X -type stabilizer generators with trivial product and h can be any vector in C_{i-1} that is not the syndrome of a Z -type error.

To give an explicit example, suppose that \mathcal{C} describes the 2D toric code with periodic boundaries and the usual stabilizer generators (X -type star operators and Z -type plaquette operators). This code has two encoded qubits and two non-trivial stabilizer relations as the product of all the stabilizer generators of the same type is the identity. In addition, every error syndrome must have even weight (this is sometimes called a materialized symmetry of the code [71]). Therefore, we can take $g = \mathbf{1}$ and $h = (1, 0, \dots, 0)$.

We note that one can always construct a metacheck matrix for a rank-deficient parity-check matrix. However, at least in topological codes, the metachecks are usually defined to be the relations comprising $O(1)$ stabilizer generators, i.e., the metacheck matrix has low-weight rows (and low-weight columns as it turns out). On the other hand, the spacelike invariants such as g and g' above are relations comprising an extensive number of stabilizer generators. The rationale for this distinction is that if each stabilizer measurement is noisy, then combining an extensive number of measurement outcomes will yield no useful information in the limit of large code size. Indeed, this is what makes it non-trivial to preserve the value of these logical correlations in QEC protocols.

Let us also comment explicitly on the case of a single-shot CSS code with rank-deficient parity-check matrices that is completely described by a length-2 chain complex. Here, there is no explicit notion of metachecks. As noted above, metachecks can be constructed based on the linear dependencies in the parity-check matrices. The resulting metacheck matrices can be interpreted as classical codes with distances d_{M_X} and d_{M_Z} . Our results therefore extend to codes where d_{M_X} and d_{M_Z} are non-trivial.

1. Fault distances

The fault distances of \mathcal{F} can essentially be read off Eqs. (B7) and (B10), but we provide a derivation here for completeness. For an arbitrary length-1 chain complex \mathcal{R} , Zeng and Pryadko showed in Ref. [14] that the

product complex $\mathcal{F} = \mathcal{R} \times \mathcal{C}$ has homological distances

$$\begin{aligned} d_j(\mathcal{F}) &= \min[d_0(\mathcal{R})d_i(\mathcal{C}), d_1(\mathcal{R})d_{i-1}(\mathcal{C})], \\ d_j(\mathcal{F}^T) &= \min[d_0(\mathcal{R}^T)d_j(\mathcal{C}^T), d_1(\mathcal{R}^T)d_{j-1}(\mathcal{C}^T)], \end{aligned} \quad (\text{B12})$$

where $d_j(\mathcal{C})$ ($d_j(\mathcal{F}^T)$) is equal to the weight of the minimal weight operator in the (co)homology group $H_j(\mathcal{C})$ ($H^j(\mathcal{C})$). For \mathcal{R} above we have

$$\begin{aligned} d_0(\mathcal{R}) &= d_1(\mathcal{R}^T) = 1, \\ d_1(\mathcal{R}) &= d_0(\mathcal{R}^T) = \delta, \end{aligned} \quad (\text{B13})$$

where δ is the length of the repetition code. Therefore the primal and dual distances of \mathcal{F} are

$$\begin{aligned} d_i &= \min[d_i(\mathcal{C}), \delta d_{i-1}(\mathcal{C})], \\ d_{i+1} &= \min[\delta d_{i+1}(\mathcal{C}^T), d_i(\mathcal{C}^T)]. \end{aligned} \quad (\text{B14})$$

Appendix C: Single-shot decoding for fault complexes

Here we give further details on the decoding of fault complexes with the single-shot property and explain a key difference between the fault complex and CBQC pictures of single-shot decoding.

We consider the fault complex $\mathcal{F} = \mathcal{R} \times \mathcal{C}$, where \mathcal{R} describes a distance ℓ repetition code with the parity-check matrix R and \mathcal{C} is a length-4 chain complex describing a CSS code with meta-checks. For a CSS code of this type, we have

$$\begin{aligned} H_X &= \partial_2^C, & H_Z^T &= \partial_3^C, \\ M_X &= \partial_1^C, & M_Z^T &= \partial_4^C, \end{aligned} \quad (\text{C1})$$

where M_X and M_Z denote the meta-check matrices for X and Z checks, respectively.

Recall that the fault complex is formally a length-5 chain complex

$$\mathcal{C} = C_5 \xrightarrow{\partial_5} C_4 \xrightarrow{\partial_4} C_3 \xrightarrow{\partial_3} C_2 \xrightarrow{\partial_2} C_1 \xrightarrow{\partial_1} C_0, \quad (\text{C2})$$

with boundary maps given by

$$\partial_j = \left(\begin{array}{c|c} \mathbb{1}_r \otimes \partial_j^C & R \otimes \mathbb{1}_{n_{j-1}} \\ \hline 0 & \mathbb{1}_c \otimes \partial_{j-1}^C \end{array} \right). \quad (\text{C3})$$

We identify the primal and dual qubits with the vector spaces C_2 and C_3 , respectively. Hence, the graph state connectivity is specified by ∂_3 , while the primal and dual detectors are given by $D_X = \partial_2$ and $D_Z = \partial_4^T$, respectively.

Per the main text, this fault complex has no ‘‘meta-detectors’’ and can be reduced to a length-3 sub-complex without any loss of information. To understand why this is the case, first notice that the detector matrices D_X and D_Z already contain fault locations, using the terminology of CBQC, of data and ancilla faults. This can be

seen by constructing, e.g., the matrix D_X for $\delta = 2$ and performing column and row operations

$$D_X = \begin{pmatrix} M_X & & & & & \\ \mathbb{1} & H_X & \mathbb{1} & & & \\ & & M_X & & & \\ & & \mathbb{1} & H_X & \mathbb{1} & \\ & & & & & M_X \end{pmatrix}. \quad (\text{C4})$$

In the above matrix, the odd rows detect ancilla faults and the even rows detect data faults, while odd columns are ancilla fault locations and even columns are data fault locations. Unlike in the CBQC framework for single-shot error correction, in the fault complex picture, there is no distinction between data faults and ancilla faults, or equivalently between detectors arising from stabilizers (H_X) and detectors arising from meta-checks (M_X). Thus, for any error e_X with syndrome $s_X = D_X e_X$ we have $\partial_1 s_X = \partial_1 \partial_2 e_X = 0$.

In Eq. (C4) we have also highlighted two blocks. The first block (teal) is the relevant check matrix for a single round of the overlapping window decoder, specifying a single detector block in the overlapping window decoder for $w = 1$. The second block (red) is identical to the single-stage decoding matrix proposed in Ref. [22]. This block can be recovered from block one by treating the ancilla faults from the previous round (first column of block one) as perfect, which eliminates them from the decoding problem. The full block is the relevant detector check matrix for a window size $w = 2$.

Appendix D: Numerical simulations

Here we describe in more detail how the simulations are performed to obtain the sustainable thresholds of the 3D and 4D toric codes. All simulations in the manuscript were performed using a private version of FlamingPy [72].

1. Phenomenological noise

We begin by describing the case of phenomenological noise. Since we are only considering a single type of Pauli error in our simulations, we only need to decode a single side of the fault complex. First, we construct the associated fault complex through foliation based on the base code, e.g., the 3D toric code, over δ rounds. In the cluster state picture, this corresponds to a cluster state of $2\delta + 1$ layers. As we are using 30 iterations of the minimum belief propagation (BP) algorithm, potentially followed by ordered statistics decoding post-processing with an order-60 combination sweep (CS-60) search strategy, we do not require the gauge group generators. Given the dual detectors D_Z , we sample faults corresponding to each matrix column from an i.i.d noise model with probability p . Any faults occurring on the initial and final layer are removed to assert that we are starting and

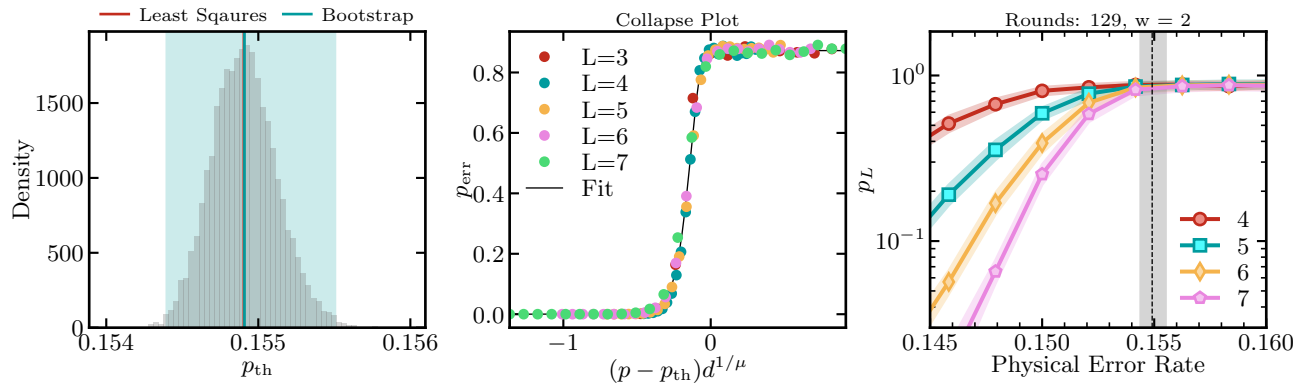


FIG. 4. Example of the threshold fitting procedure for the 3D toric code under the photonic GKP noise model with an $w = 2$ overlapping window decoder after 129 rounds of noisy syndrome measurements. **Left:** Histogram of the bootstrap resamples, with the mean and 99% confidence interval highlighted in blue. **Center:** Collapse plot of the fitted data. **Right:** Threshold plot of the data obtained from the sustainable threshold simulation with the threshold value highlighted as a black dashed line and 99% confidence intervals as a grey shading.

ending in a code state. This assumption is equivalent to the usual assumption in the phenomenological noise model simulations that the final syndrome measurement is noise-free. For each trial, the sampled fault vector is sliced up according to the $(w, 1)$ -overlapping window decoder before being passed to the local decoder. A more explicit description of this can be found in Refs [48, 50]. After the full correction c_δ over δ rounds is calculated, we check whether the residual error is a logical error. For the 3D and 4D toric codes that possess 3 and 6 logical qubits, we count as a failure if at least a single logical qubit remains in error.

2. Photonic GKP noise

When simulating Xanadu’s photonic architecture based on optical Gottesman-Kitaev-Preskill qubits [1, 2, 4], a few adjustments to the simulation routine are necessary. First, as we are aiming to simulate an approximation of the physical noise model, we now require knowledge about the bi-adjacency matrix of the (qubit-level) fault-tolerant graph state. As described in Ref. [4], using the process of *macronization* and *stitching* the qubit-level graph state can equivalently be described by several GKP Bell pairs and linear-optical circuit elements, e.g., phase shifters and beam splitters. For each optical mode describing a GKP state, we sample a random displacement from the normal distribution $\mathcal{N}(0, \sigma^2)$ with variance σ^2 . This is an effective model to describe a finite-energy GKP quanaught state with $-10 \log_{10}(\sigma^2/\sigma_{\text{vac}}^2)$ dB of per-peak squeezing, where we set the vacuum variance $\sigma_{\text{vac}}^2 = 2$. As described in more detail in Refs. [1, 2, 4], the sampled displacements can be processed to yield measurement outcomes for the individual modes when they are measured in the *reduction* step described in Ref. [4]. From this, an effective qubit-level noise model can be obtained and the

rest of the simulation routine continues as described in the previous section.

3. Threshold estimation

The common way of obtaining an estimate of the threshold based on the simulation of finite system sizes consists of performing a quadratic fit with the rescaled error rate [73, 74], that is,

$$x = (p - p_{th})d^{1/\mu}, \quad (\text{D1})$$

$$f(x) = ax^2 + bx + c, \quad (\text{D2})$$

with p_{th} the threshold to be fitted, d the code distance, μ a scaling parameter and a, b, c free parameters of the quadratic polynomial. However, this approach cannot be followed for determining the threshold estimate of sustainable threshold simulations. For a sufficiently large number of decoding rounds, the observed logical error rate will saturate at $p_L = 1 - (0.5)^k$ in the vicinity of the threshold, i.e., for $p \approx p_{th}$. Thus, it is impossible to observe a threshold as a crossing of curves for finite system sizes: this crossing lies in a region where the error rates saturate. To capture accurately the behavior described above, we consider fitting to an alternative model, that is,

$$g(x) = a \left[1 - \left(1 - \frac{1 + \tanh(bx)}{2} \right)^c \right], \quad (\text{D3})$$

where x is the rescaled error rate as in Eq. (D1) and a, b, c are free fit parameters. In principle, if the fit is performed over a sufficient range of x , one does not need to fit a and can set it instead to its analytical value $a \equiv 1 - (0.5)^k$; however, we leave a as a free parameter. The parameter c typically scales with the number of decoding rounds.

To estimate the threshold based on the model Eq. (D3), we use the bootstrap resampling technique with 10000 resamples; see [75] for an implementation. The obtained (asymmetric) error bars represent the 99% confidence intervals. Fig. 4 contains some example plots for the threshold fitting procedure.

4. Stability experiments

In the 3D toric code stability experiments described in the End Matter of the main text, we observe the expected behaviour for a fixed code and increasing window size. Namely, we observe exponential suppression of the logical error rate below threshold; see Fig. 5.

Appendix E: Fault complexes of subsystem codes

Here, we briefly discuss the extension of our fault complex formalism to subsystem codes [65–67]. We recall that a CSS subsystem code is defined by two (gauge) matrices G_X and G_Z , but unlike in the subspace code case, we do not require that $G_X G_Z^T = 0$ [76]. The X -type stabilizers of the subsystem code are the elements of the row space of G_X that have even overlap all rows of G_Z , and vice versa for the Z -type stabilizers. We use the notation H_X and H_Z for the X - and Z -type stabilizer matrices, respectively.

Prior work on foliation [9, 10, 77] gives us clues for the

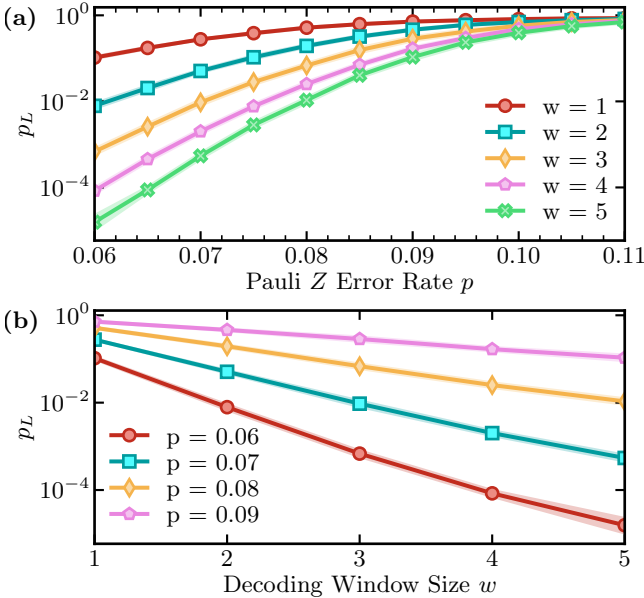


FIG. 5. Stability experiments with the $L = 5$ 3D toric code. (a) Logical error rate as a function of the Pauli error rate p for various sizes of the decoding window w . (b) Scaling of the logical error rate below the threshold as a function of the size of the decoding window w .

correct form of the fault complexes of subsystem codes. We know that in a foliated CSS subsystem code the ancilla qubit connections correspond to the rows of G_X and G_Z and the data qubits connections are unchanged. This suggests that—for a length-3 fault complex—the boundary operator ∂_2 describing the cluster state connectivity should be as in Eq. (C3) with $\partial_i^C = G_Z^T$ and $\partial_{i-1}^C = G_X$. However, for the other boundary operators, we should use H_X and H_Z instead of G_X and G_Z , as subsystem code detectors are formed from the stabilizers not the checks. Explicitly,

$$D_X = \partial_1 = \left(\mathbb{1}_r \otimes H_X \mid R \otimes \mathbb{1}_{n_0} \right), \quad (\text{E1})$$

$$\partial_2 = \left(\begin{array}{c|c} \mathbb{1}_r \otimes G_Z^T & R \otimes \mathbb{1}_{n_1} \\ \hline 0 & \mathbb{1}_c \otimes G_X \end{array} \right), \quad (\text{E2})$$

$$D_Z^T = \partial_3 = \left(\begin{array}{c} R \otimes \mathbb{1}_{n_2} \\ \hline \mathbb{1}_c \otimes H_Z^T \end{array} \right). \quad (\text{E3})$$

For the case of CSS subsystem codes with meta-checks, we expect that D_X and D_Z would simply need to include M_X and M_Z (the meta-check matrices) and would resemble Eq. (C4). Given the similarity of the detector matrices, the decoding problem for these codes should be identical in structure to the decoding problem for fault complexes we have previously covered. It would be therefore interesting to examine the performance of, e.g., subsystem codes with single-shot error correction [36, 45, 68, 78] using the approach explored in this work.

The changes outlined above are relatively minor and we therefore anticipate foliated CSS subsystem codes can be represented naturally as fault complexes. The main barrier to formalizing our intuition is finding the appropriate representation of CSS subsystem codes as chain complexes (see [68, 79] for some possibilities). We leave this for future work.

Appendix F: Fault complexes of circuit models

In Ref. [32], Li proposes a low-density parity-check representation of fault-tolerant quantum circuits. The formalism introduced there can be seen as another perspective of space-time codes; see also Refs. [27, 28, 30, 80]. In Sec. VIII of [32], the author gives explicit expressions obtained from their formalism for operations that do not couple X and Z type operators, resulting in two disjoint Tanner graphs. In particular, they obtain the matrix representation, for what we call the gauge group generators, as

$$G_X = \left(\begin{array}{cc} \mathbf{a}_X \otimes \mathbb{1}_n & \mathbb{1}_{m_X^c} \otimes \mathbf{H}_X^T \\ \mathbf{d}_X^T \otimes H_Z & 0 \end{array} \right), \quad (\text{F1})$$

$$G_Z = \left(\begin{array}{cc} \mathbf{a}_Z \otimes \mathbb{1}_n & \mathbb{1}_{m_Z^c} \otimes \mathbf{H}_Z^T \\ \mathbf{d}_Z^T \otimes H_X & 0 \end{array} \right), \quad (\text{F2})$$

where m_X^C (m_Z^C) denotes the number of rows of \mathbf{a}_X (\mathbf{a}_Z), the detector matrices are given by

$$D_X = \left(\mathbb{1}_{m_X^B} \otimes H_X \quad \mathbf{a}_X^T \otimes \mathbb{1}_{r_X} \right), \quad (\text{F3})$$

$$D_Z = \left(\mathbb{1}_{m_Z^B} \otimes H_Z \quad \mathbf{a}_Z^T \otimes \mathbb{1}_{r_Z} \right), \quad (\text{F4})$$

and logical operators as

$$L_X = (\mathbf{g}_X \otimes \ell_X), \quad (\text{F5})$$

$$L_Z = (\mathbf{g}_Z \otimes \ell_Z), \quad (\text{F6})$$

Here, the quantities \mathbf{a}_X and \mathbf{d}_X are specific to the concrete circuit, however, they already have large similarity

with matrices obtained from the hypergraph product of a length-2 chain complex with a length-1 complex.

More evidence that our formalism can also describe fault-tolerant error correction is found by considering the explicit example of the r -times repeated measurement of stabilizer generators. This example is discussed in Sec. VII C of Ref. [32]. For this example, translating the notation of Li to our notation, \mathbf{a}_X is the check matrix of the repetition code and g_X is the all-one vector, equivalent to what we have obtained in Section B from the Künneth formula. The matrix \mathbf{d}_X is equivalent to the r -dimensional identity matrix $\mathbb{1}_r$ up to an additional all-zero row. Similar expressions are obtained when expressing D_Z and L_Z .

-
- [1] J. E. Bourassa, R. N. Alexander, M. Vasmer, A. Patil, I. Tzitrin, T. Matsuura, D. Su, B. Q. Baragiola, S. Guha, G. Dauphinais, K. K. Sabapathy, N. C. Menicucci, and I. Dhand, Blueprint for a scalable photonic fault-tolerant quantum computer, *Quantum* **5**, 392 (2021), [arXiv:2010.02905](#).
- [2] I. Tzitrin, T. Matsuura, R. N. Alexander, G. Dauphinais, J. E. Bourassa, K. K. Sabapathy, N. C. Menicucci, and I. Dhand, Fault-tolerant quantum computation with static linear optics, *PRX Quantum* **2**, 040353 (2021), [arXiv:2104.03241](#).
- [3] S. Bartolucci, P. Birchall, H. Bombín, H. Cable, C. Dawson, M. Gimeno-Segovia, E. Johnston, K. Kieling, N. Nickerson, M. Pant, F. Pastawski, T. Rudolph, and C. Sparrow, Fusion-based quantum computation, *Nat Commun* **14**, 912 (2023).
- [4] B. W. Walshe, B. Q. Baragiola, H. Ferretti, J. Gefaell, M. Vasmer, R. Weil, T. Matsuura, T. Jaeken, G. Pantaleoni, Z. Han, T. Hillmann, N. C. Menicucci, I. Tzitrin, and R. N. Alexander, *Linear-optical quantum computation with arbitrary error-correcting codes* (2024), [arXiv:2408.04126 \[quant-ph\]](#).
- [5] H. J. Briegel, D. E. Browne, W. Dür, R. Raussendorf, and M. Van den Nest, Measurement-based quantum computation, *Nature Phys* **5**, 19 (2009).
- [6] R. Raussendorf and J. Harrington, Fault-tolerant quantum computation with high threshold in two dimensions, *Phys. Rev. Lett.* **98**, 190504 (2007).
- [7] N. Nickerson and H. Bombín, *Measurement based fault tolerance beyond foliation* (2018), [arXiv:1810.09621 \[quant-ph\]](#).
- [8] M. Newman, L. A. de Castro, and K. R. Brown, Generating fault-tolerant cluster states from crystal structures, *Quantum* **4**, 295 (2020).
- [9] A. Bolt, G. Duclos-Cianci, D. Poulin, and T. M. Stace, Foliated quantum error-correcting codes, *Phys. Rev. Lett.* **117**, 070501 (2016).
- [10] B. J. Brown and S. Roberts, Universal fault-tolerant measurement-based quantum computation, *Phys. Rev. Research* **2**, 033305 (2020).
- [11] A. M. Steane, Error correcting codes in quantum theory, *Phys. Rev. Lett.* **77**, 793 (1996).
- [12] A. R. Calderbank and P. W. Shor, Good quantum error-correcting codes exist, *Phys. Rev. A* **54**, 1098 (1996).
- [13] J.-P. Tillich and G. Zémor, Quantum ldpc codes with positive rate and minimum distance proportional to the square root of the blocklength, *IEEE Trans. Inf. Theory* **60**, 1193 (2014).
- [14] W. Zeng and L. P. Pryadko, Higher-dimensional quantum hypergraph-product codes with finite rates, *Phys. Rev. Lett.* **122**, 230501 (2019).
- [15] H. Bombin and M. A. Martin-Delgado, Homological error correction: Classical and quantum codes, *Journal of Mathematical Physics* **48**, 052105 (2007).
- [16] N. P. Breuckmann and J. N. Eberhardt, Quantum low-density parity-check codes, *PRX Quantum* **2**, 040101 (2021).
- [17] M. B. Hastings, Weight reduction for quantum codes, *Quantum Info. Comput.* **17**, 1307 (2017), [arXiv:1611.03790 \[quant-ph\]](#).
- [18] S. Evra, T. Kaufman, and G. Zémor, Decodable quantum ldpc codes beyond the \sqrt{n} distance barrier using high-dimensional expanders, *SIAM J. Comput.*, *FOCS20* (2022).
- [19] E. Dennis, A. Kitaev, A. Landahl, and J. Preskill, Topological quantum memory, *J. Math. Phys.* **43**, 4452 (2002).
- [20] M. Vasmer and D. E. Browne, Three-dimensional surface codes: Transversal gates and fault-tolerant architectures, *Phys. Rev. A* **100**, 012312 (2019).
- [21] A. O. Quintavalle, M. Vasmer, J. Roffe, and E. T. Campbell, Single-shot error correction of three-dimensional homological product codes, *PRX Quantum* **2**, 020340 (2021).
- [22] O. Higgott and N. P. Breuckmann, Improved single-shot decoding of higher-dimensional hypergraph-product codes, *PRX Quantum* **4**, 020332 (2023), [arXiv:2206.03122 \[quant-ph\]](#).
- [23] C. Gidney, Stability experiments: The overlooked dual of memory experiments, *ArXiv2204.13834 Quant-Ph* (2022), [arXiv:2204.13834 \[quant-ph\]](#).
- [24] D. Gottesman, *Stabilizer codes and quantum error correction* (1997), [arXiv:quant-ph/9705052](#).
- [25] C. Gidney, Stim: a fast stabilizer circuit simulator, *Quantum* **5**, 497 (2021), [arXiv:2103.02202](#).
- [26] P.-J. H. S. Derks, A. Townsend-Teague, A. G. Burchards, and J. Eisert, *Designing fault-tolerant circuits using detector error models* (2024), [arXiv:2407.13826 \[quant-ph\]](#).
- [27] D. Gottesman, *Opportunities and challenges in fault-*

- tolerant quantum computation (2022), [arXiv:2210.15844 \[quant-ph\]](#).
- [28] N. Delfosse and A. Paetzniak, [Spacetime codes of clifford circuits](#) (2023), [arXiv:2304.05943 \[quant-ph\]](#).
- [29] H. Bombin, C. Dawson, T. Farrelly, Y. Liu, N. Nickerson, M. Pant, F. Pastawski, and S. Roberts, [Fault-tolerant complexes](#) (2023), [arXiv:2308.07844 \[quant-ph\]](#).
- [30] X. Fu and D. Gottesman, [Error correction in dynamical codes](#) (2024), [arXiv:2403.04163 \[quant-ph\]](#).
- [31] M. E. Beverland, S. Huang, and V. Kliuchnikov, [Fault tolerance of stabilizer channels](#) (2024), [arXiv:2401.12017 \[quant-ph\]](#).
- [32] Y. Li, [Low-density parity-check representation of fault-tolerant quantum circuits](#) (2024), [arXiv:2403.10268 \[quant-ph\]](#).
- [33] R. Raussendorf, S. Bravyi, and J. Harrington, Long-range quantum entanglement in noisy cluster states, *Phys. Rev. A* **71**, 062313 (2005).
- [34] D. Horsman, A. G. Fowler, S. Devitt, and R. V. Meter, Surface code quantum computing by lattice surgery, *New J. Phys.* **14**, 123011 (2012).
- [35] D. Litinski, A game of surface codes: Large-scale quantum computing with lattice surgery, *Quantum* **3**, 128 (2019).
- [36] H. Bombin, Single-shot fault-tolerant quantum error correction, *Phys. Rev. X* **5**, 031043 (2015).
- [37] E. T. Campbell, A theory of single-shot error correction for adversarial noise, *Quantum Sci. Technol.* **4**, 025006 (2019).
- [38] O. Fawzi, A. Grospellier, and A. Leverrier, Constant overhead quantum fault-tolerance with quantum expander codes, in *2018 IEEE 59th Annu. Symp. Found. Comput. Sci. FOCS* (2018) pp. 743–754.
- [39] S. Gu, E. Tang, L. Caha, S. H. Choe, Z. He, and A. Kubica, Single-shot decoding of good quantum ldpc codes, *Commun. Math. Phys.* **405**, 85 (2024).
- [40] I. Dinur, M.-H. Hsieh, T.-C. Lin, and T. Vidick, [Good quantum ldpc codes with linear time decoders](#) (2022), [arXiv:2206.07750 \[quant-ph\]](#).
- [41] A. Leverrier and G. Zémor, [Quantum tanner codes](#) (2022), [arXiv:2202.13641 \[quant-ph\]](#).
- [42] P. Pantelev and G. Kalachev, Asymptotically good quantum and locally testable classical ldpc codes, in *Proc. 54th Annu. ACM SIGACT Symp. Theory Comput., STOC 2022* (Association for Computing Machinery, New York, NY, USA, 2022) pp. 375–388.
- [43] N. P. Breuckmann and J. N. Eberhardt, Balanced product quantum codes, *IEEE Trans. Inf. Theory* **67**, 6653 (2021).
- [44] M. B. Hastings, J. Haah, and R. O’Donnell, Fiber bundle codes: breaking the $n^{1/2}$ polylog(n) barrier for quantum ldpc codes, in *Proc. 53rd Annu. ACM SIGACT Symp. Theory Comput., STOC 2021* (Association for Computing Machinery, New York, NY, USA, 2021) pp. 1276–1288.
- [45] B. J. Brown, N. H. Nickerson, and D. E. Browne, Fault-tolerant error correction with the gauge color code, *Nat Commun* **7**, 12302 (2016).
- [46] L. Skoric, D. E. Browne, K. M. Barnes, N. I. Gillespie, and E. T. Campbell, Parallel window decoding enables scalable fault tolerant quantum computation, *Nat Commun* **14**, 7040 (2023), [arXiv:2209.08552 \[quant-ph\]](#).
- [47] L. Berent, T. Hillmann, J. Eisert, R. Wille, and J. Roffe, Analog information decoding of bosonic quantum low-density parity-check codes, *PRX Quantum* **5**, 020349 (2024).
- [48] S. Huang and S. Puri, Increasing memory lifetime of quantum low-density parity check codes with sliding-window noisy syndrome decoding, *Phys. Rev. A* **110**, 012453 (2024).
- [49] H. Bombin, C. Dawson, Y.-H. Liu, N. Nickerson, F. Pastawski, and S. Roberts, [Modular decoding: parallelizable real-time decoding for quantum computers](#) (2023), [arXiv:2303.04846 \[quant-ph\]](#).
- [50] T. R. Scruby, T. Hillmann, and J. Roffe, [High-threshold, low-overhead and single-shot decodable fault-tolerant quantum memory](#) (2024), [arXiv:2406.14445 \[quant-ph\]](#).
- [51] P. Pantelev and G. Kalachev, Degenerate quantum ldpc codes with good finite length performance, *Quantum* **5**, 585 (2021).
- [52] J. Roffe, D. R. White, S. Burton, and E. Campbell, Decoding across the quantum low-density parity-check code landscape, *Phys. Rev. Res.* **2**, 043423 (2020).
- [53] N. P. Breuckmann, K. Duivenvoorden, D. Michels, and B. M. Terhal, Local decoders for the 2d and 4d toric code, *Quantum Info. Comput.* **17**, 181–208 (2017).
- [54] N. P. Breuckmann and X. Ni, Scalable Neural Network Decoders for Higher Dimensional Quantum Codes, *Quantum* **2**, 68 (2018).
- [55] K. Duivenvoorden, N. P. Breuckmann, and B. M. Terhal, Renormalization group decoder for a four-dimensional toric code, *IEEE Trans. Inf. Theory* **65**, 2545 (2019).
- [56] A. Kubica, *The ABCs of the Color Code: A Study of Topological Quantum Codes as Toy Models for Fault-Tolerant Quantum Computation and Quantum Phases Of Matter*, Ph.D. thesis, Caltech (2018).
- [57] M. Vasmer, D. E. Browne, and A. Kubica, Cellular automaton decoders for topological quantum codes with noisy measurements and beyond, *Scientific Reports* **11**, 2027 (2021).
- [58] A. B. Alosious and P. K. Sarvepalli, Decoding toric codes on three dimensional simplicial complexes, *IEEE Transactions on Information Theory* **67**, 931 (2021).
- [59] D. Gottesman, A. Kitaev, and J. Preskill, Encoding a qubit in an oscillator, *Phys. Rev. A* **64**, 012310 (2001).
- [60] T. Hillmann, L. Berent, A. O. Quintavalle, J. Eisert, R. Wille, and J. Roffe, [Localized statistics decoding: A parallel decoding algorithm for quantum low-density parity-check codes](#) (2024), [arXiv:2406.18655 \[quant-ph\]](#).
- [61] T. R. Scruby and K. Nemoto, Local probabilistic decoding of a quantum code, *Quantum* **7**, 1093 (2023), [arXiv:2212.06985 \[quant-ph\]](#).
- [62] N. Berthussen, J. Dreiling, C. Foltz, J. P. Gaebler, T. M. Gatterman, D. Gresh, N. Hewitt, M. Mills, S. A. Moses, B. Neyenhuis, P. Siegfried, and D. Hayes, [Experiments with the 4d surface code on a qccd quantum computer](#) (2024), [arXiv:2408.08865 \[quant-ph\]](#).
- [63] D. Bluvstein and others, Logical quantum processor based on reconfigurable atom arrays, *Nature* **626**, 58 (2024).
- [64] H. Zhou, C. Zhao, M. Cain, D. Bluvstein, C. Ducker, H.-Y. Hu, S.-T. Wang, A. Kubica, and M. D. Lukin, [Algorithmic fault tolerance for fast quantum computing](#) (2024), [arXiv:2406.17653 \[quant-ph\]](#).
- [65] D. Kribs, R. Laflamme, and D. Poulin, Unified and generalized approach to quantum error correction, *Phys. Rev. Lett.* **94**, 180501 (2005).
- [66] D. W. Kribs, R. Laflamme, D. Poulin, and M. Lesosky,

- Operator quantum error correction, *Quantum Info. Comput.* **6**, 382 (2006).
- [67] D. Poulin, Stabilizer formalism for operator quantum error correction, *Phys. Rev. Lett.* **95**, 230504 (2005).
- [68] A. Kubica and M. Vasmer, Single-shot quantum error correction with the three-dimensional subsystem toric code, *Nat. Commun.* **13**, 6272 (2022).
- [69] P. Panteleev and G. Kalachev, Quantum ldpc codes with almost linear minimum distance, *IEEE Trans. Inf. Theory* **68**, 213 (2022).
- [70] One can think of this parity-check matrix as being the vertex-to-edge adjacency matrix of the cycle graph.
- [71] B. J. Brown, Conservation laws and quantum error correction: Toward a generalized matching decoder, *IEEE BITS Inf. Theory Mag.* **2**, 5 (2022), [arXiv:2207.06428](https://arxiv.org/abs/2207.06428) [cond-mat, physics:quant-ph].
- [72] FlamingPy repository, <https://github.com/XanaduAI/flamingpy>.
- [73] C. Wang, J. Harrington, and J. Preskill, Confinement-higgs transition in a disordered gauge theory and the accuracy threshold for quantum memory, *Annals of Physics* **303**, 31 (2003).
- [74] J. W. Harrington, *Analysis of Quantum Error-Correcting Codes: Symplectic Lattice Codes and Toric Codes*, Ph.D. thesis, California Institute of Technology (2004).
- [75] Threshold bootstrap code, <https://gist.github.com/chubbbc/59f7dcb8d5d6f7a1a8f5ccc237c8d61d>.
- [76] M. L. Liu, N. Tantivasadakarn, and V. V. Albert, Subsystem CSS codes, a tighter stabilizer-to-CSS mapping, and Goursat’s Lemma, *Quantum* **8**, 1403 (2024).
- [77] A. Bolt, D. Poulin, and T. M. Stace, Decoding schemes for foliated sparse quantum error-correcting codes, *Phys. Rev. A* **98**, 062302 (2018).
- [78] C. Stahl, Single-shot quantum error correction in intertwined toric codes, *Phys. Rev. B* **110**, 075143 (2024).
- [79] W. Zeng and L. P. Pryadko, Minimal distances for certain quantum product codes and tensor products of chain complexes, *Phys. Rev. A* **102**, 062402 (2020).
- [80] D. Bacon, S. T. Flammia, A. W. Harrow, and J. Shi, Sparse quantum codes from quantum circuits, *IEEE Trans. Inf. Theory* **63**, 2464 (2017).